A solid state electrochemical device for studying thermodynamic and transport properties of non-stoichiometric oxides: Application to ceria

Philippe Garcia, Marlu Cesar Steil, Audrey Miard, Erwin Douguet-Bronnec, Franck Fournet-Fayard, Jacques Fouletier

dateDecember 31, 2020

A solid state electrochemical device for studying thermodynamic and transport properties of non-stoichiometric oxides: application to ceria

Philippe Garcia[a], Marlu Cesar Steil[b], Audrey Miard[a], Erwin Douguet–Bronnec[a], Franck Fournet–Fayard[b], Jacques Fouletier[b]

[a] *CEA, DES, IRESNE, DEC, Cadarache F-13108 Saint-Paul-Lez-Durance, France*
[b] *Univ. Grenoble Alpes, CNRS, Grenoble INP, LEPMI, 38000 Grenoble, France, Univ. Savoie Mont Blanc, Grenoble, France*

Abstract

An electrochemical tool for characterising properties of non–stoichiometric oxides is described that is based on Electromotive Force (E.M.F.) measurements and coulometric titration. The tool may be used to subject samples to either solid–state or gas phase redox perturbations. A theoretical analysis of the setup shows that the open–circuit voltage (OCV) is characteristic of the oxygen activity in the solid at the interface between the sample and the Yttria Stabilised Zirconia (YSZ) sample–holder in the case of an inhomogeneous, essentially electronic conducting material. The device's purpose is illustrated with a study of cerium oxide at 900°C. By running simple solid state reduction experiments, it is possible to simultaneously derive thermodynamic and chemical diffusion data consistent with existing literature. The approach we present appears as an interesting alternative to other techniques such as the relaxation method or impedance spectroscopy.

Keywords: cerium oxide, non–stoichiometry, Nernst equation, coulometric titration, chemical potential of oxygen, chemical diffusion, defect behaviour
PACS: 82.45.Xy, 82.33.Pt, 66.30.Ny

1. Introduction

Non–stoichiometric oxides such as ceria or urania have a wide range of energy applications. Ceria for instance, is considered in a solar thermochemical cycle enabling the dissociation of either CO_2 or H_2O for fuel production[1]. This

Email addresses: philippe.garcia@cea.fr (Philippe Garcia), marlu-cesar.steil@lepmi.grenoble-inp.fr (Marlu Cesar Steil), audrey.miard@cea.fr (Audrey Miard), erwin.douguet-bronnec@cea.fr (Erwin Douguet–Bronnec), franck.fournet-fayard@grenoble-inp.fr (Franck Fournet–Fayard), jacques.fouletier@lepmi.grenoble-inp.fr (Jacques Fouletier)

occurs through a two–stage process involving reduction at high temperature and oxidation at lower temperature of the non–stoichiometric material. Ceria is also an alternative to YSZ for use as an electrolyte or electrode material operating at lower temperatures in electrochemical devices, especially solid oxide fuel cells (SOFC)[2]. Urania or urania–based mixed oxides constitute another class of important non–stoichiometric functional materials as they are the most widely used, easily manufactured fuels for fission reactors. Many of these materials' engineering properties are modified as a result of oxygen non–stoichiometry and migration which occurs under the combined effects of electrochemical potential and temperature gradients.

Coulometric titration and E.M.F. measurements have for many decades now, proven themselves to be very useful tools to determine bulk thermodynamic properties [3, 4]. However, to optimise these mixed ionic electronic conducting (MIEC) materials and eventually control the associated industrial processes through modelling or other means, requires a detailed knowledge of a number of fundamental thermodynamic and atomic transport properties relative to bulk or surface behaviour. It is the aim of this paper to illustrate how some of these properties may be investigated using a combination of E.M.F. measurements, coulometric titration and gas phase equilibration. The solid–state electrochemical device we developed is applied to the study of sintered ceria, and we seek to establish whether the methodology, *i.e.* the device itself and the data analysis, provides quantitative estimates of both kinetic and thermodynamic material properties. We particularly endeavour to determine the device's usefulness in regard to oxygen diffusion properties. Indeed, as is the case for uranium dioxide [5], data relative to this property are notoriously scattered for reasons relating either to the microstructure of samples, the experimental method adopted, the data analysis, often a combination of all three.

The paper is organised as follows. Section 2 is devoted to a description of the device along with an analysis of the physical significance of the quantities measured during a redox experiment. In section 4, we present a number of experimental results relative to redox experiments either through the gas phase or the solid state. The data were acquired at 900°C. The discussion section (section 5) focuses successively on the equilibrium and transient data we derive in the course of this study.

2. Device description and theoretical analysis of measured physical quantities

2.1. Device description

Figure 1 shows a schematic cross–section of the central part of the device. The high temperature region of the cell comprises two alumina tubes (items (1a) and (1c)) which make up two gas–tight compartments separated by a YSZ membrane. Two O–rings guarantee that no gas may permeate between the upper and lower compartments or from outside of these regions. An argon circulation is maintained in the volume between the outer alumina cylinder (item

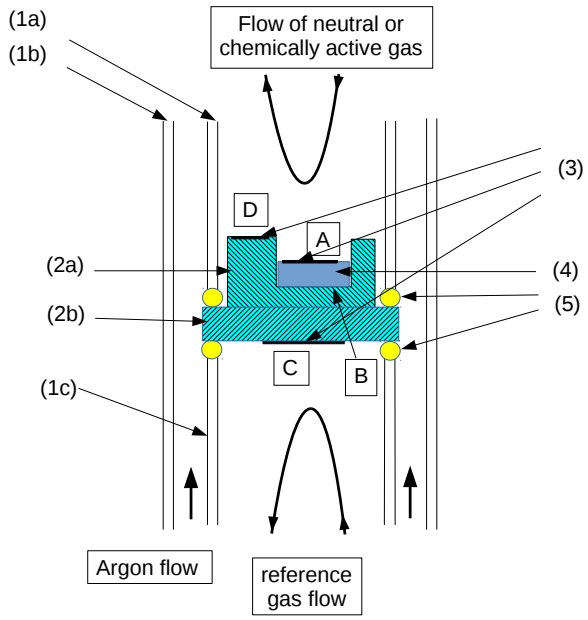

Figure 1: Schematic cross–section of device: (1a) upper alumina tube; (1b) outer alumina tube; (1c) lower alumina tube; (2a) YSZ sample holder; (2b) YSZ membrane; (3)platinum deposits; (4) MIEC sample; (5) gold O–rings. A, B, C and D refers to the points between which electrical potentials are measured (A, C, D) or enter into the analysis (B).

(1b)) and the cylindrical structure comprising the upper and lower alumina cylinders separated by the YSZ membrane. This further safeguards against any oxygen permeation from outside. The device is positioned in the isothermal region of a Pyrox furnace. The temperature the system may reach is estimated at 1400°C. It is not necessary to describe the device in its entirety. Suffice it to say that a gas circulation can be established in the upper section of the cell containing either a controlled mixture of argon and oxygen or a mixture of hydrogen, water vapour and argon thus enabling to buffer the entire system. The gas is directed directly onto the sample via a small allumina capillary.

The oxygen partial pressures are modified by controlling the carrier gas (argon or mixture of argon and 5% hydrogen) flow rates and/or by enriching or depleting the carrier gas of oxygen using a so–called electrochemical pump [6, 7]. Oxygen pressure measurements are carried out upstream and downstream from the sample using air–reference solid state gauges [8]. Both input and output gauges are maintained at 680°C. In a similar manner, a constant flow rate of argon and oxygen or industrial air is established in the lower device–compartment which provides a reference for the E.M.F. measurements. The oxygen partial pressure of the gas is prescribed and monitored. Finally, two thermocouples are used to monitor the sample temperature. One is placed very close to the sample surface in the upper compartment of the device. The second is placed against the lower face of the YSZ membrane (item (2b)).

2.2. E.M.F. in the case of a homogeneous MIEC and coulometric titration

Three platinum leads connected to points A, C and D are extracted from the device and the potential difference between points A and C and D and C are acquired continuously. The E.M.F or Nernst potential of the cells may be written as:

$$U_M - U_C = \frac{\mathrm{R}T}{4\mathscr{F}}\mathrm{Ln}(\frac{p_{O_2}^M}{p_{O_2}^C}) \tag{1}$$

Where M stands for points A or D and therefore $p_{O_2}^M$ represents the oxygen activity of the gas phase (if $M = D$) or of the solid (if $M = A$), T is the homogeneous temperature of the device, R and $\mathscr{F}$ are the ideal gas and Faraday constants respectively. Relationship (1) (see for instance [9]) only applies under the following conditions:

- thermodynamic equilibrium is reached at both electrodes, *i.e.* at the interface between the metal of electrode A and the MIEC on the one hand (or the triple junction in D) , and between the triple junction in C comprising the electrode, the ionic conductor (item (2b) in Figure 1) and the gas phase on the other.
- the electrolytes (items (2a) and (2b) in Figure 1) are ideal ionic conductors.
- the MIEC studied is homogeneous.
- the temperature of the device is homogeneous.

- the metal deposits (item (3) in Figure 1)) are made of identical materials.

If the circuit between A and C is closed and for instance a negative value of $U_A - U_C$ is imposed, then a current circulates through it and one may expect that oxygen is transferred from the MIEC to the ionic conductor through the interface between the two solids. Oxygen ions recombine at point C to form oxygen molecules. Common caveats may stem from imposing too negative a potential drop which may lead to a reduction of the YSZ or from residual oxygen being present in the gas phase and contributing to the measured current. Assuming these caveats are not relevant, the stoichiometry variation of the MIEC as a result of such a reduction (or oxidation) sequence is given by:

$$\Delta x = \frac{M_{CeO_2}}{2\mathscr{F} m_{CeO_2}} \times \int_{t_1}^{t_2} i(u)du \tag{2}$$

In this relationship, Δx represents the variation of the absolute value of deviation from stoichiometry of the solid between t_1 and t_2, $i(u)$ is the current circulating through the electrical circuit at time u, m_{CeO_2} is the mass of the sample at exact stoichiometry and M_{CeO_2} is the molar mass of stoichiometric material. Note that the condition above that items (2a) and (2b) (YSZ in our case) be ideal ionic conductors is essential here for equation 2 to apply as these features of the set–up serve to guarantee that no electrons are transferred to or from the MIEC through the circuit.

2.3. E.M.F. in the case of an inhomogeneous MIEC

The previous section provides a straightforward means of determining the fundamental relationship between composition and oxygen partial pressure: one starts off at a known deviation from stoichiometry and subjects the sample to repeated reduction sequences, each followed by a relaxation period sufficiently long for the E.M.F. to stabilise. More novel is to derive the expression for $U_A - U_C$ when there exists an oxygen gradient in the MIEC in a direction perpendicular to the surface. One assumes that the only charged mobile species in the MIEC and YSZ (items (2a) and (2b)) are negatively charged oxygen ions (O^{-2}) and electrons (e'). More assumptions must be made, namely all of those of the previous section bar the homogeneity of the MIEC. In addition, we postulate that at all times, there is no discontinuity of the electrochemical potential of oxygen ions across the interface at point B. Under such conditions, application of Wagner theory leads to the following expression for $U_A - U_C$:

$$U_A - U_C = \frac{\mathrm{R}T}{4\mathscr{F}} \int_{B_{miec}}^{A} t_{O^{2-}} \times d(Ln(p_{O_2})) + \frac{\mathrm{R}T}{4\mathscr{F}} \mathrm{Ln}\left(\frac{p_{O_2}^{B_{miec}}}{p_{O_2}^{C}}\right) \tag{3}$$

In this expression, B_{miec} represents a point located in the MIEC at interface B and $t_{O^{2-}}$ is the ionic number of the MIEC, *i.e.*, the ratio of ionic conductivity of the material over its total conductivity. Three limiting cases may be discussed:

- if the MIEC is homogeneous, the left–hand side integral vanishes and one may write that $p_{O_2}^{B_{miec}} = p_{O_2}^{A}$, in which case Nernst's expression (1) is recouped.

- if the MIEC is essentially an electronic conductor, then the value of $U_A - U_C$ is related to the oxygen activity at the interface between the sample and YSZ, provided there is no polarization phenomenon at interface B:

$$U_A - U_C = \frac{\mathrm{R}T}{4\mathscr{F}} \mathrm{Ln}\left(\frac{p_{O_2}^{B_{miec}}}{p_{O_2}^{C}}\right) \tag{4}$$

- if the MIEC is essentially an ionic conductor, then the value of $U_A - U_C$ is related to the oxygen activity at the upper surface of the sample:

$$U_A - U_C = \frac{\mathrm{R}T}{4\mathscr{F}} \mathrm{Ln}\left(\frac{p_{O_2}^{A}}{p_{O_2}^{C}}\right) \tag{5}$$

2.4. Set–up advantages

Various set–ups have been proposed which combine coulometric titration and E.M.F. measurements (see for instance the review paper of Patrakeev and co–workers [10]) and its sensitivity is noticeably greater than that of thermogravimetry (*ca.* 10^{-8} against 10^{-6} moles of O_2). However, the coulometric method often requires carefully sealing the different cell compartments. The main sources of error are indeed the result of gas leaks which are either due to the physical permeation of oxygen through the sealing of the various cell components or to the semi–permeability of oxygen across the electrolyte walls. The use of a double–walled cell substantially reduces measurement errors: the sample holder is set on a YSZ membrane and consequently, the oxygen semi–permeation flux across it can be reduced by adjusting the oxygen partial pressure on the reference side of the cell. Moreover, as demonstrated previously [8], the oxygen semi–permeability flux does not reach the interface between the sample and the YSZ sample–holder (interface B in Figure 1) thus circumventing the polarization phenomenon which constitutes a source of error. Another difficulty of these methods is the measurement of the oxygen pressure in the gas in the vicinity of the sample which the monitoring of $U_A - U_C$ deals with in the present case.

3. Material used and experimental conditions

The cerium oxide sample we studied was manufactured through a powder metallurgy process. Powders 99.95% were obtained from Janssen Chimica. The powder was subjected to uniaxial pressing followed by isostatic pressing at 2500 bars. The resulting cylindrical pellets were sintered at 1450°C for two hours, following which the material density was about 88% of its theoretical value. The diameter and thickness of the sintered sample were approximately 7.7 mm and 2.6 mm respectively and its mass was roughly 0.85 g. The upper surface of the

sample was then covered in a layer of platinum paint and subsequently cured at 900°C for half an hour in air.

Two distinct sets of measurements were carried out at 900°C using a reference gas with an oxygen partial pressure of either 88×10^{-6} atm. for the solid–state reduction or 0.21 atm. (air) for the gas–phase reduction experiments. The former reference value was obtained by passing a small current through an electrochemical pump located at the entrance of the lower cell compartment. Solid state reduction experiments were carried out in an 166 ml/min flow of purified argon.

4. Experimental results

4.1. Solid state reduction

4.1.1. Observations and tentative interpretation

A typical experiment consists in initially oxidising the sample in an argon flow enriched in oxygen using the electrochemical oxygen pump upstream from the upper–cell and then subjecting the sample to a set of reduction and relaxation sequences. Figure 2 shows a typical set of reduction and relaxation sequences. The reduction of the sample is brought about by polarising the cell, *i.e.* by imposing a potential difference between points A and C (see Figure 1) of $\approx$ -1.7 V in this particular case. We checked by measuring $U_A - U_C$ just after a reduction phase that this value was never less than -1 V, thus guaranteeing that the YSZ membrane was not reduced and that the quantity of oxygen derived through equation 2 was due to oxygen depletion in the sample or the gas phase (residual oxygen) only.

Figure 2 indicates that the cell voltage equilibrates at roughly -22.5 $\pm$0.2 mV prior to any reduction. By extrapolating the experimental data of Panelener [11] and coworkers to the appropriate oxygen pressure one may estimate the sub–stoichiometry of the sample at 10^{-5}. Once the cell voltage has stabilised, the oxygen initially present in the carrier gas is eliminated completely. Despite this however, the air–reference oxygen probe indicates an output oxygen pressure of approximately 2.6×10^{-6} atm. prior to any relaxation period. This is due to the fact that the connections between the steel and alumina pipes which feed the gas to the upper cell–compartment are not perfectly gas tight.

Figure 2 may be used to discuss three recurrent features:

- The relaxation period comprises two distinct stages. The OCV increases rapidly immediately after the reduction period. It subsequently increases more slowly to values which are much lower than the initial cell voltage indicating that the sample has been substantially reduced. This slow increase is consistent with the presence of residual oxygen in the upper–cell compartment.

- Consistent with the previous observation, as the first reduction period begins, the output probe voltage deceases from *circa.* -232 mV to -251 mV and remains at roughly this value so long as the sample remains sub–stoichiometric.

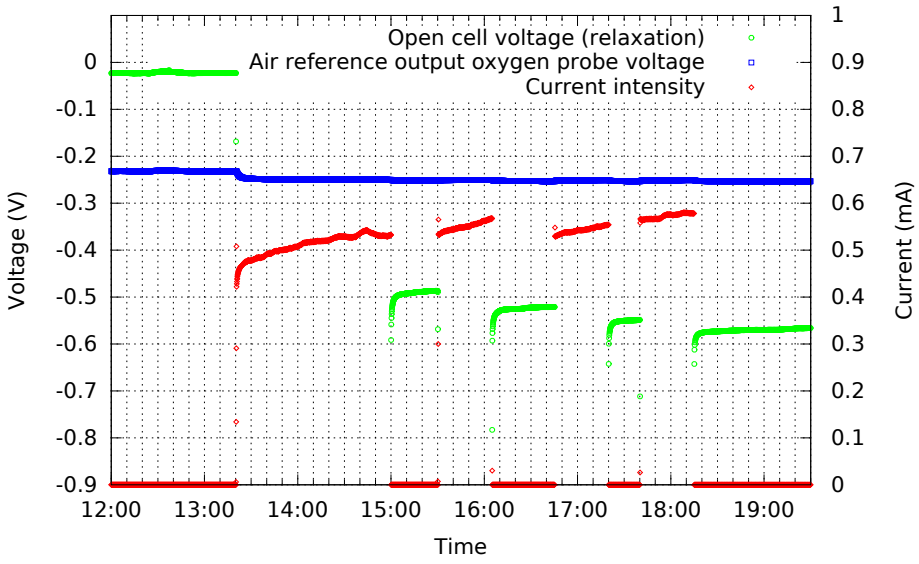

Figure 2: Set of four reduction and relaxation sequences, starting from stoichiometric CeO_2. Green circles indicate the change in cell voltage whereas blue squares correspond to air–reference output oxygen probe voltage.

- Although not illustrated explicitly in Figure 2, if one waits long enough, the cell voltage eventually increases until the sample reoxidises completely. Only then does it reach a stable value.

One may suggest an interpretation of the above observations as follows. During the reduction process, oxygen is driven out of the sample through the sample/YSZ interface and eventually recombines at point C. The rate at which this occurs is given by the current circulating in the circuit which itself is externally controlled via the $U_A - U_C$ potential drop. If oxygen from the bulk of the sample does not arrive at a fast enough rate then one would expect an oxygen gradient to be set up between the interface and the bulk of the sample. Recall from section 2.3, that the OCV of an electronic conducting non–stoichiometric oxide provides the oxygen activity at the interface between the solid state electrolyte and the sample. Hence, this rule applies to sub–stoichiometric cerium oxide (see for instance [12] and references therein). Once the reduction process ceases, the open cell voltage increases sharply as the oxygen concentration reaches a new steady–state distribution and the gradient established during the reduction period vanishes. This would explain the first phase of the relaxation period.

The residual oxygen present in the gas phase is absorbed by the sample both during the reduction period and the relaxation period at the surface exposed to the gas circulating in the upper–cell compartment. During the reduction period, this quantity of oxygen contributes to the integrated current as used,

via equation 2, to determine the stoichiometry change in the sample between the beginning and the end of the reduction sequence. The rate at which oxygen is driven out of the gas phase in this way is basically given by the difference between the residual oxygen flow rate in the gas phase prior to any reduction and the residual oxygen flow rate following the first reduction. We can estimate this rate as corresponding to approximately 1.6×10^{-6}atm. for our gas flow rate. In determining the change in stoichiometry of the sample, one must of course account for this correction. During the relaxation period, as oxygen is absorbed at the sample surface and the average oxygen concentration in the solid rises, the OCV gradually increases at a rate controlled by the absorption rate and oxygen diffusion coefficient. This explains the second stage of the relaxation period during which the OCV rises at a slower rate.

Based on this analysis, we endeavour to quantify thermodynamic and diffusion data in the following subsections.

4.1.2. Determination of thermodynamic data

In coulometric titration experiments, one data point corresponds to the change in stoichiometry of a sample as it changes from one oxygen activity to another. So, if the oxygen partial pressure increment is sufficiently small, one in effect is measuring the derivative of the oxygen partial pressure of the sample with respect to deviation from stoichiometry. The integration of this function (assuming an integration constant is known, *i.e.*, a value of the oxygen partial pressure at which x is known *a priori*) then provides the desired relationship. This requires determining the changes in non–stoichiometry for sufficiently small oxygen partial pressure increments. A more practical way of proceeding is to assume that within a sufficiently narrow oxygen partial pressure range, deviation from stoichiometry follows a power law of the oxygen partial pressure. With the knowledge of the initial and final oxygen partial pressures, the problem then becomes to identify the exponent and pre–factor of the law. Note that the initial oxygen activity of the sample is derived from relationship (4). We only assume at this stage that the sample has a virtually homogeneous oxygen concentration. The quantity of oxygen which the sample has lost is given by equation (2), corrected for the caveat highlighted in section 4.1.1 . There remains to determine the final sample oxygen activity, *i.e.*, the oxygen activity immediately following the reduction. One may surmise that if the oxygen diffusion coefficient were infinitely high, the value of the open–circuit voltage would rise so quickly that only the second stage of the relaxation period (see section 4.1.1), *i.e.*, corresponding to the linear increase with time of the OCV illustrated in Figure 2, would be observed. Therefore, a reasonable estimate of the oxygen activity in the sample immediately following the reduction process is obtained from a linear extrapolation of the OCV to the time at which the relaxation process begins.

Figure 3 shows a comparison between the calculated increments of deviation from stoichiometry, assuming this quantity to be a power law function of the oxygen pressure, and the corresponding measured quantities. The power law

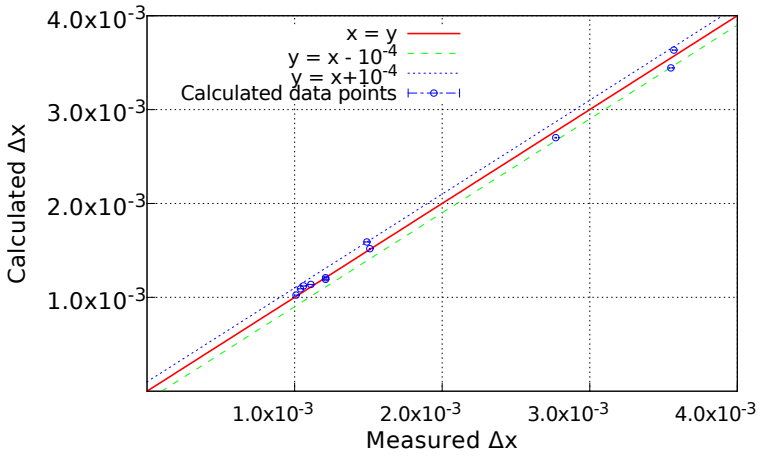

Figure 3: Calculated *vs.* measured deviation from stoichiometry increments. Calculated values are obtained assuming a power law relationship between oxygen partial pressure and deviation from stoichiometry. The power law coefficients are obtained from a least squares fit: $x = 4.6 \pm 0.5 \times 10^{-6} p_{O2}^{0.222 \pm 0.004}$

parameters are obtained from a least squares fit between modelled and experimental data. We find that:

$$x = A p_{O2}^{\alpha} = 4.6(\pm 0.5) \times 10^{-6} p_{O2}^{0.222 \pm 0.004} \tag{6}$$

In Figure 3, in addition to the $x = y$ line, we have included two additional straight lines each separated from $x = y$ by 10^{-4}. This latter value provides an estimate of the uncertainty with which deviation from stoichiometry can be determined with our experimental setup. It corresponds to a sensitivity in terms of O_2 molecules of roughly 3×10^{-7} moles which is compatible with other such values reported in the literature [10].

4.1.3. Determination of kinetic data

In order to interpret the transient, relaxation data, we have modelled both these stages using Fick's second law applied to the description of oxygen diffusion within the sample. The idea is to solve this partial differential equation, calculate the oxygen distribution at any given time throughout the sample, so in particular at the interface between the sample and the YSZ sample holder. Using the thermodynamic data determined in the preceding paragraph, one may further derive the oxygen activity at the interface, hence, using Nernst's law, a numerical equivalent to the OCV. The conservation of oxygen atoms within the samples during a reduction or relaxation period, may be written as follows:

$$\frac{\partial C}{\partial t} = \nabla.(\widetilde{D}_O \nabla C) \tag{7}$$

where C is the time and space dependent oxygen concentration, and $\widetilde{D}_O$ the oxygen chemical diffusion coefficient. If the majority point defect population

is responsible for oxygen diffusion throughout the experiment, then the oxygen chemical diffusion is proportional to the defect diffusion coefficient and equation 7 may further be simplified by assuming a uniform diffusion coefficient. This follows from the application of Darken's equation (see for instance [13], p. 210) on the condition that diffusion on the cation sublattice is negligible in comparison to diffusion on the anion sublattice. The results from the previous section (deviation from stoichiometry follows a power law of the oxygen pressure) point to the fact that a single type of oxygen defect is present under the conditions relevant to our experiments.

The sample is modelled as a one-dimensional structure (horizontal slabs of uniform concentration) and all exchange of oxygen ions is assumed to occur homogeneously on the upper sample surface, directly facing the Ar gas flow, or on the lower sample surface, at the interface between the YSZ and the sample.

In accordance with comments made in the previous section, the sample is assumed homogeneous prior to a given reduction experiment. Initial conditions to equation (7), are provided by the oxygen concentration as measured from the OCV prior to reduction and application of equations (1) and (6) . We assume variable flux boundary conditions on both faces of the sample. On its upper face, *i.e.* that directly exposed to the carrier gas, we assume that the sample absorbs a quantity of oxygen which corresponds roughly to the difference between the output fluxes prior to and following the initial reduction (equivalent to approximately 1.6×10^{-6}atm., section 4.1.1):

$$\widetilde{D}_O \left(\frac{\partial C}{\partial z}\right)_{top} S = \frac{2 g_f}{P V_{mol}} (p^0_{O2} - p^1_{O2}) \tag{8}$$

where $\left(\frac{\partial C}{\partial z}\right)_{top}$ is the oxygen concentration gradient on the upper surface of the sample, S is the upper surface area of the sample, P is the total gas pressure in the carrier gas (1 atm.), V_{mol} is the molar volume of the carrier gas (24 l mol^{-1}) and g_f is the argon flow rate. During a relaxation period, there is no oxygen flux across the YSZ–sample interface so that the oxygen concentration gradient is zero, whereas during a reduction period, oxygen is driven out of the sample through the interface at a rate provided by the cell current at time t. The resulting boundary condition is expressed as:

$$\widetilde{D}_O \left(\frac{\partial C}{\partial z}\right)_{bot} S = \frac{i(t)}{2\mathscr{F}} \tag{9}$$

Equation (7) is solved assuming boundary conditions (9) and (8) using an explicit finite difference numerical scheme. At each time step the local deviation from stoichiometry is calculated at each axial location and, in particular, at the YSZ–sample interface, whence a model value of the OCV is derived. A Lenvenberg–Marquardt algorithm (see for instance [14]) for nonlinear least squares problems is implemented in such a way that for each reduction experiment, values of the chemical diffusion coefficient of oxygen, $\widetilde{D}_O$, and power–law pre–factor A (see 6) are determined that minimise the difference between exper-

imental and calculated values of the OCV. The results of such a minimisation procedure are illustrated in Figure 4.

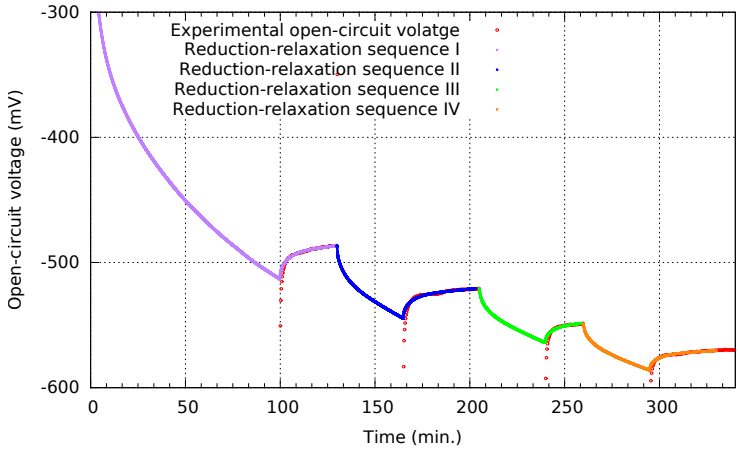

Figure 4: Calculated *vs.* measured OCV for the four consecutive reduction experiments illustrated in Figure 2. Calculated values result from an optimisation procedure that enables the determination of the power law pre–factor (equation 2) and the oxygen chemical diffusion coefficient $\widetilde{D}_O$.

4.2. Gas phase reduction

4.2.1. Experiments and preliminary interpretation

This type of experiment, aimed at measuring kinetic related data, involves equilibrating a non–stoichiometric oxide under conditions of constant temperature and oxygen partial pressure and subsequently subjecting it to more oxidising or reducing conditions whilst monitoring a property sensitive the sample's oxygen content. This property is typically either mass through thermogravimetric experiments or ionic or electronic conductivity. Initially, the oxygen concentration at the sample surface changes and then progressively through the bulk until eventually the oxygen distribution is homogeneous. Such an experiment is sensitive to two physical quantities: the rate at which oxygen diffusion proceeds in the sample bulk, *i.e.* related to the oxygen chemical diffusion coefficient, and the rate at which oxygen is absorbed at the sample surface from the gas phase through some surface exchange phenomenon. Qualitatively speaking, two limiting cases may exist depending upon whether one or the other phenomenon is rate limiting. If diffusion and oxygen incorporation proceed at very slow and fast rates respectively, then the change in property will be exclusively sensitive to oxygen chemical diffusion. The reverse is of course true if surface exchange is sluggish in comparison to chemical diffusion. Ideally though, both kinetics are roughly equivalent and the experiment is sensitive to both physical quantities (see for instance reference [15]).

The CeO_2 sample was thus maintained at *circa* 900°C in a flow of Ar (167 ml/min) and, starting from different values of non–stoichiometry (the experiment lasted several weeks), the conditions were changed by adding either 20, 40 or 80 ml/min of a mixture of Ar and 5% H_2. In addition to modifications in the hydrogen content, the electrochemical device upstream from the sample was used to inject oxygen corresponding to between 50 and 200 mA of current in order to produce a gas mixture which was buffered by the $H_2O(\text{vap.}) \rightleftharpoons H_2 + \frac{1}{2}O_2$ reaction.

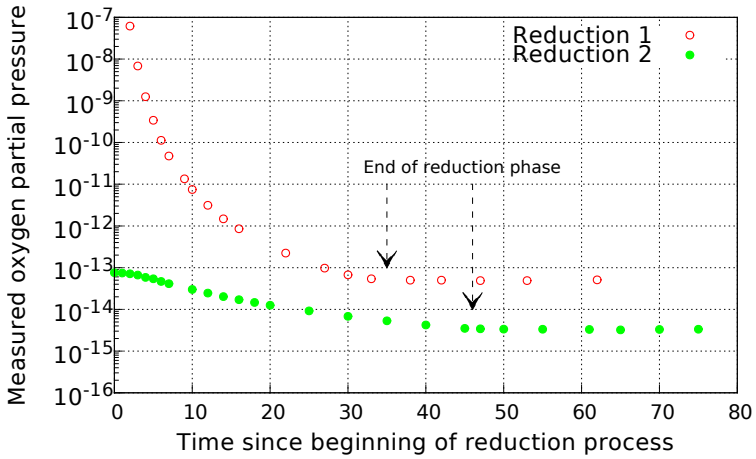

Figure 5: Change in sample oxygen pressure at 900°C derived from the cell E.M.F. following addition to the argon flow (167 ml/min) of 20 ml/min of Ar 5% H_2 and oxygen molecules corresponding to roughly 80 mA of current in YSZ pump upstream from the cell.

Figure 5 shows the change in oxygen partial pressure in the solid following prolonged exposure to argon and a sudden addition of 20 ml/min of Ar 5% H_2 and roughly 0.31 ml/min of O_2. This mixture corresponds to an oxygen potential of approximately 1.5×10^{-16} atm. Note that these curves are characteristic of all reduction or oxidation experiments we have carried out. They indicate that the oxygen partial pressure in the solid at the interface between the sample and the YSZ sample holder begins to decrease immediately following the change to a buffered reducing gas mixture. However, as soon as the reduction process ends and the sample is exposed to an argon flow, the E.M.F. of the cell stabilises to whatever value it had reached. Actually, if one maintains the argon flow for a sufficiently long period of time, the cell E.M.F. rises slowly again as already noted in section 4.1.1 as a result of oxygen ingress. The fact that the E.M.F. virtually stabilises immediately following the return to a relatively pure argon flow demonstrates that there is no subsequent redistribution of oxygen within the sample. In other words, the sample is homogeneous and one may surmise that the changes in oxygen partial pressure measured during the reduction process such as those indicated in Figure 5, are indicative of the homogeneous oxygen activity within the sample. These experiments presented here may therefore be

expected to be sensitive to the oxygen exchange coefficient only.

4.2.2. Quantitative interpretation of the data

We now demonstrate that these redox experiments may indeed provide values for the oxygen exchange coefficient k between the gas phase and the ceria surface using very simple data analysis procedures. The exchange coefficient k determines the boundary condition for the diffusion problem we wish to solve. It is defined by an alternative relation to equation (8) which models first order reaction rate kinetics at the sample surface:

$$\widetilde{D}_O \left(\frac{\partial C}{\partial z} \right)_{GSI} = -k(C_S - C_G) \tag{10}$$

In this expression, C_S and C_G represent the oxygen concentration at the surface of the solid and in the gas phase. Actually, the latter quantity corresponds to the oxygen concentration the solid would have if it were equilibrated with a gas phase at that gas phase's oxygen partial pressure. The GSI subscript indicates the relevant gradient is that at the gas–solid interface. Analytical solutions to diffusion equation exist (7) in the form of an infinite series, assuming the above boundary conditions at either end of a slab of thickness L, a homogeneous initial oxygen distribution in the solid and a uniform and constant diffusion coefficient. An expression for the average oxygen concentration is given by:

$$\frac{\bar{C}(t) - C_G}{C_i - C_G} = 2h^2 \sum_{\nu=0}^{\nu=\infty} \frac{exp(-\alpha_n^2 \widetilde{D}_O t)}{\alpha_n^2 (Lh/2 + L^2\alpha_n^2/4 + L^2h^2/4)} \tag{11}$$

expression in which C_i is the initial uniform oxygen concentration in the solid, $h = \frac{k}{\widetilde{D}_O}$ and α_n is a real number solution to the transcendental equation: $tan(\alpha_n \frac{L}{2}) = \frac{h}{\alpha_n}$. We now restrain (11) to its first order expansion, which is equivalent to a long–time solution to the problem, and further assume that h is infinitely small. In this case, it is easy to see that α_0 is given by $\alpha_0^2 \frac{L}{2} \approx h$ which, substituted into equation (11) finally yields the following simplified relationship:

$$\frac{\bar{C}(t) - C_G}{C_i - C_G} \approx exp(-\frac{2k}{L}t) \tag{12}$$

We assume equation (6) provides an accurate description of the relationship between deviation from stoichiometry and oxygen partial pressure in the range where our gas phase redox experiments are carried out. Therefore combining (6) and (12) yields:

$$r(t) = \frac{\bar{C}(t) - C_G}{C_i - C_G} = \frac{p^{\alpha}_{O_2}(t) - (p^{\alpha}_{O_2})_G}{(p^{\alpha}_{O_2})_i - (p^{\alpha}_{O_2})_G} \approx exp(-\frac{2k}{L}t) \tag{13}$$

where α has been evaluated in section 4.1.2 at 0.222. Note also that the value of $(p^{\alpha}_{O_2})_G$ is actually determined from experiment based on the application of

Experiment number	p_{O_2} of gas phase	Initial p_{O_2} of solid	Final p_{O_2} of solid	Estimated p_{H_2O}	Estimated k (ms^{-1})
1	$1.1\ 10^{-15}$	$4.6\ 10^{-15}$	$2.0\ 10^{-15}$	$4.4\ 10^{-3}$	$2.5 \pm 0.05\ 10^{-7}$
2	$1.1\ 10^{-15}$	$3.7\ 10^{-15}$	$2.1\ 10^{-15}$	$4.4\ 10^{-3}$	$2.3 \pm 0.05\ 10^{-7}$
3	$1.4\ 10^{-16}$	$1.1\ 10^{-15}$	$5.3\ 10^{-16}$	$3.2\ 10^{-3}$	$1.7 \pm 0.05\ 10^{-7}$
4	$2\ 10^{-16}$	$6.6\ 10^{-16}$	$3.7\ 10^{-16}$	$3.4\ 10^{-3}$	$1.5 \pm 0.05\ 10^{-7}$
5	$2.9\ 10^{-16}$	$9.1\ 10^{-17}$	$2.2\ 10^{-16}$	$3.6\ 10^{-3}$	$1.5 \pm 0.02\ 10^{-7}$
6	$2.7\ 10^{-16}$	$5.6\ 10^{-17}$	$8.7\ 10^{-17}$	$3.5\ 10^{-3}$	$1.5 \pm 0.07\ 10^{-7}$
7	$2.9\ 10^{-17}$	$1.7\ 10^{-16}$	$8.7\ 10^{-17}$	$2.2\ 10^{-3}$	$1.2 \pm 0.02\ 10^{-7}$
8	$3.2\ 10^{-17}$	$2.2\ 10^{-16}$	$9.4\ 10^{-17}$	$3.9\ 10^{-3}$	$1.8 \pm 0.03\ 10^{-7}$
9	$2.6\ 10^{-17}$	$1.2\ 10^{-16}$	$5.4\ 10^{-17}$	$6.1\ 10^{-3}$	$2.3 \pm 0.03\ 10^{-7}$
10	$1\ 10^{-16}$	$4.5\ 10^{-16}$	$1.6\ 10^{-16}$	$2.8\ 10^{-3}$	$1.4 \pm 0.02\ 10^{-7}$
11	$9\ 10^{-4}$	$1.7\ 10^{-16}$	$1.8\ 10^{-12}$	-	

Table 1: Set of conditions relating to all gas–phase redox experiments carried out and data analysis results. Column 1: value of the oxygen partial pressure imposed upon the solid via the gas phase; column 2: oxygen partial pressure in solid prior to experiment; column 3: oxygen partial pressure in solid immediately after the experiment, in an inert gas environment; column 4: estimated water vapour pressure during redox experiment; column 5: estimated oxygen solid–gas surface exchange coefficient, at 900°C, obtained from linear regression analysis of data points.

Nernst's law to the quantity $U_D - U_A$ (see section 2.2). We further checked that the *in situ* measured oxygen partial pressure in the gas phase (*i.e.*, $(p_{O_2})_G$) actually corresponded to within 10 % of the expected value under the relevant experimental conditions (Ar and H_2 flow rates, current circulating through the electrochemical pump and temperature).

Table 1 reports the experimental conditions under which the redox experiments were carried out, *i.e.*, the oxygen partial pressure in the gas phase during the experiment; the starting, supposedly homogeneous, oxygen activity in the solid; the oxygen activity in the solid at the end of the reduction or oxidation process; and the water vapour pressure calculated assuming the above–mentioned buffering reaction.

Figure 6 reports in a semi–logarithmic representation the change in r values with time during the reduction sequences for experiments 1 and 2 in Table 1. They were carried out on different days but under practically identical conditions and the figure therefore illustrates reproducibility of experiments. More importantly, the data points, as with all but one of the experiments from Table 1, fall roughly along a straight line indicating that the simple model described above is relevant: the gas–solid oxygen exchange coefficient is constant and may indeed be derived from these experiments.

5. Discussion

5.1. Equilibrium data

Figure 7 shows a comparison of the equilibrium data reported in this study with that of previous authors [11, 16, 17] at similar temperatures.

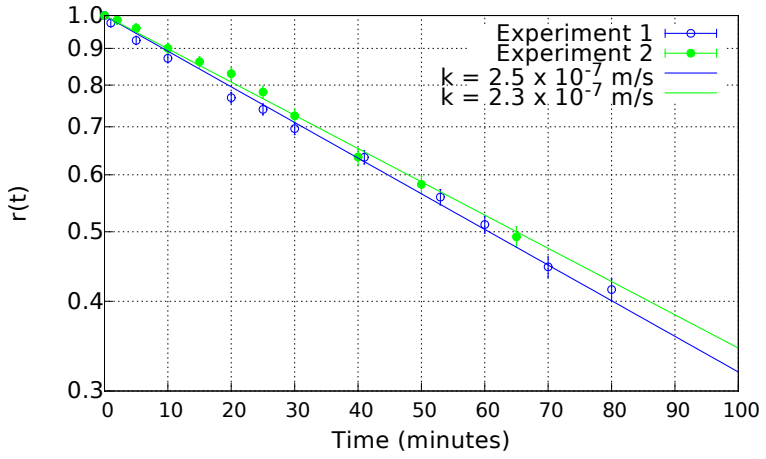

Figure 6: Change in sample $r(t)$ (equation 13) at 900°C derived from cell E.M.F. measurements, following addition to the argon flow (167 ml/min) of 20 ml/min of Ar 5% H_2 and oxygen molecules corresponding to roughly 107 mA of current through the YSZ pump upstream from the cell.

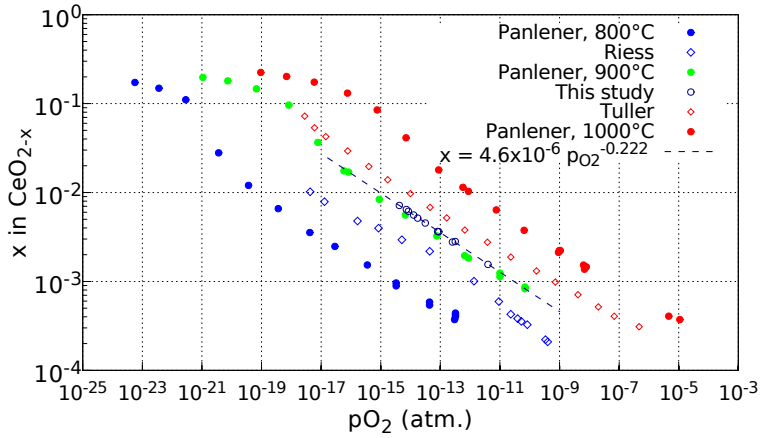

Figure 7: Deviation from stoichiometry values as a function of oxygen partial pressure reported in this study compared to those reported in the past using different techniques (thermogravimetry [11], coulometric titration [18], analysis of electrical conductivity data [17]).

The figure shows that the values we report are closer to those obtained using a thermogravimetric technique at the same temperature by Panlener *et al.* [11] than those reported by Tuller and Nowick [17] who based their estimates on electrical conductivity measurements. The oxygen partial pressure exponents (α) however are close in all three studies and correspond to values of roughly $\frac{-1}{5}$ ($\frac{-1}{4.5\pm0.1}$ in the present case). One would expect from simple point defect theory that, for pure CeO_{2-x} assuming non–interacting defects, $\alpha \approx \frac{-1}{6}$. Some authors have claimed that this inconsistency may be the sign of the presence of singly charged oxygen vacancies but Dawicke and Blumenthal [19] suggested, based on electrical conductivity measurements which also showed a -1/5 oxygen partial pressure exponent, that this was due to a charge compensation effect resulting from the presence of doubly ionized calcium ions. Whatever the exact cause of this deviation from the expected behaviour of pure ceria, the values we have obtained fully justify the use of $\alpha \approx \frac{-1}{4.5}$ in our data analysis of the transient data.

5.2. Transient data

5.2.1. Solid state reductions: diffusion coefficients

Diffusion coefficients were determined by applying the data analysis procedure presented in section 4.1.3. The data were reproduced by the model as satisfactorily as shown in Figure 4 indicating the relevance of one of the main hypotheses underpinning the model: that a single anion point defect type was predominant throughout all of the diffusion experiments. Note that the deviation from stoichiometry of the sample lies below *circa* 7×10^{-3} as may be seen in Figure 7. The average diffusion coefficient determined from the eleven experiments was estimated at $1.9 \pm 0.3 \times 10^{-9}$ m^2s^{-1}.

A number of chemical diffusion coefficients or ionic mobilities have been reported in the literature [20, 21, 1, 22]. We now ascertain the extent to which the reported data are consistent with these studies focusing on the more complete sets of data of Lai and Haile [21] and Ackermann *et al.* [22]. Unfortunately, the temperature we have investigated falls in neither of the temperature ranges these two studies cover and so we resort to extrapolating these authors' data. The former investigation is based on a detailed examination of ceria doped with 15% of Sm ($Sm_{0.15}Ce_{0.85}O_{1.925-\delta}$) using impedance spectroscopy. Both electronic and ionic mobilities are reported at temperatures between 500°C and 650°C. Assuming, as is the case in pure ceria, *i.e.*, in our study, that $2[V_O^{\circ\circ}] = [e']$, the chemical diffusion coefficient may be derived, again in the dilute limit approximation, from the following expression:

$$\widetilde{D}_O = \frac{3D_{V_O^{\circ\circ}}}{(1 + \frac{\mu_i}{\mu_e})} \tag{14}$$

where $D_{V_O^{\circ\circ}}$, μ_i and μ_e are the vacancy diffusion coefficient, ionic and electronic mobilities respectively. Note that because the activation energy for electron hopping (*circa* 0.2 eV) is about three times less than the activation energy

for oxygen vacancy migration (0.6-0.7 eV), the ratio of ion to electron mobilities increases with increasing temperature to reach 0,2 at 900°C. The chemical diffusion coefficient obtained from extrapolating these data is estimated at 3.3×10^{-9} m^2s^{-1} which compares remarkably well with the value we report here: $1.9 \pm 0.3 \times 10^{-9}$ m^2s^{-1}. In contrast, the values extrapolated from the data of Ackermann *et al.* [22], obtained for a deviation from stoichiometry of 1% at high temperatures using thermogravimetric analysis and the relaxation method, are far lower than the values obtained by Lai and Haile. In particular their activation energy for chemical diffusion is in the region of 3.7 eV which is high for oxygen diffusion in such a coumpound. In addition to the deviation from stoichiometry reported being slightly lower than in our study, the relaxation method involves oxygen exchange at the surface of the sample which constitutes one potential source of confusion. Because the temperatures in Ackermann *et al.*'s study are so much higher than in ours or in that of Lai and Haile, one cannot exclude a different mechanism taking over at high temperature being the cause of this discrepancy.

5.2.2. Gas–phase redox experiments: surface exchange kinetics

Looking at the exchange coefficients of experiments 3, 4, 5 and 6 (Table 1), the following tentative conclusions may be drawn:

- the exchange coefficient may be considered constant over a range of oxygen partial pressures spanning 1.5 orders of magnitude.
- the exchange coefficient appears to be the same for the reduction or oxidation process (comparison of k values for experiments 3 and 4 (reduction experiments) on the one hand and 5 and 6 (oxidation experiments) on the other.

Experiments 7, 8 and 9 were carried out under practically identical start and finish sample and gas–phase oxygen pressures. However, we made sure by acting upon flow rates and YSZ pump currents, that the water vapour pressures were significantly different.

Figure 8 shows that the exchange coefficient increases with increasing water vapour pressure therefore demonstrating that we are dealing with a physical parameter that is not characteristic of the bulk properties of the material but rather is related to the mechanisms via which oxygen is transferred to (respectively from) the solid from (respectively to) the gas phase.

Note that not all oxidation or reduction experiments were characterised by a decreasing exponential $r(t)$ function. Experiments 10 and 11 are respectively reduction and oxidation experiments that were carried out in succession. Figure 9 shows the $r(t)$ functions (equation 13) which correspond to both these experiments.

It is noteworthy that the $r(t)$ function corresponding to experiment 11 is not a simple exponential function. The reason for this is that the oxygen partial pressure the sample is exposed to is high and it is therefore probable that it undergoes a change from electronic conduction to a mixed conducting regime as

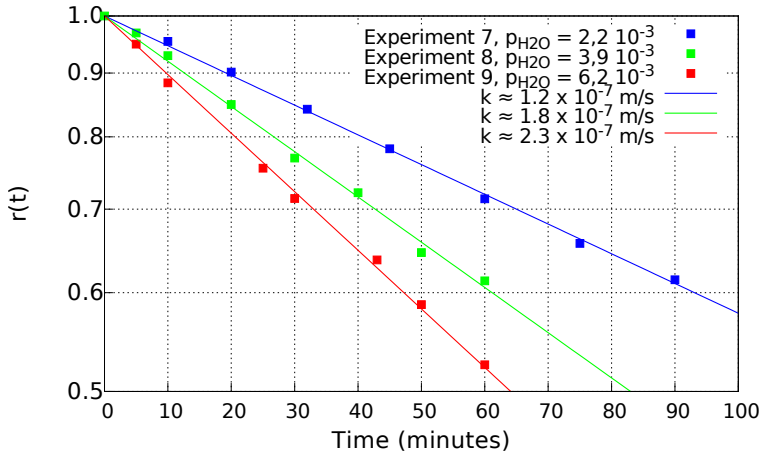

Figure 8: Logarithmic representation of $r(t)$ (equation (13)) for reduction experiments 7, 8 and 9 (Table 1) that are identical in all but the water vapour pressures they were carried out under. This confirms, if need be, that these gas–phase reduction experiments are limited by the kinetics of oxygen surface exchange and that water molecules are involved in the transfer of oxygen from the solid to the gas phase.

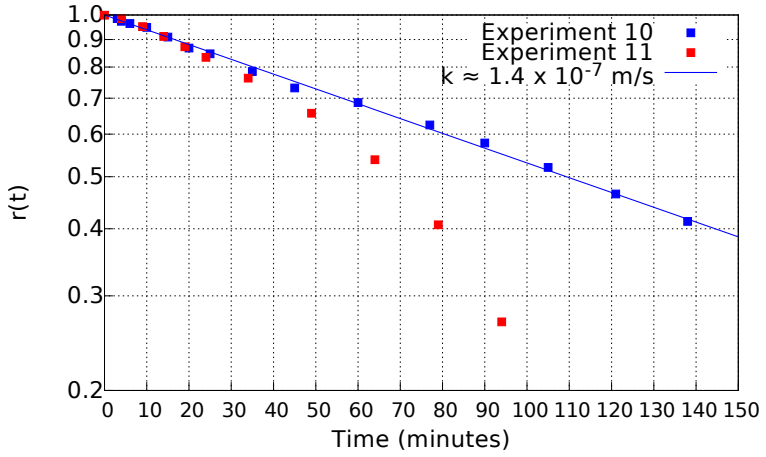

Figure 9: $r(t)$ corresponding to experiments 10 (reduction) and 11 (oxidation), see Table 1. The experiments were carried out consecutively and the figure shows that function $r(t)$ for experiment 11 is not an exponentially decreasing function of time. One possible reason for this is that all the conditions for assuming that the OCV is related through Nernst's law to the oxygen activity of the solid at the interface between the solid and the YSZ sample holder is not fulfilled (see text for details).

it approaches exact stoichiometry. As a result, the simplified analysis we allude to in section 2.3 no longer applies. It is also quite possible that at smaller deviations from stoichiometry than the ones corresponding to experiments 1 through 10, the surface exchange coefficient changes as the vacancy concentration at the sample surface decreases sharply. A more detailed analysis would be required to model a more complex experiment in its entirety.

Finally, one may wonder about the consistency between the diffusion coefficient estimate determined in section 5.2.1 and the oxygen surface exchange estimate derived from our simplified analysis. Solving the transcendental equation for $tan(\alpha_0 \frac{L}{2}) = \frac{h}{\alpha_0}$ for $h \approx \frac{2\times10^{-7}}{2\times10^{-9}}\mathrm{m}^{-1}$ yields $\alpha_0 \approx 271.5\ \mathrm{m}^{-1}$. This is within roughly 2 % of the approximated value given by $\sqrt{\frac{2h}{L}}$ and hence fully justifies the simplified expression for $r(t)$ provided by equation (13).

6. Conclusions

An electrochemical tool for characterising properties of non–stoichiometric oxides is reported that is based on E.M.F. measurements and coulometric titration. The tool provides chemical potential of oxygen data for different oxygen contents. In addition to this though, we have analysed the physical significance of the different quantities measured and in particular, the OCV: in the case of an inhomogeneous, essentially electronic conductor, this quantity corresponds to the activity in the solid at the interface between the solid and the YSZ sample–holder; in the case of an inhomogeneous, essentially ionic conductor, the OCV is a measure of the oxygen activity in the solid at its upper surface.

The data this device is capable of generating is illustrated with a study of cerium oxide at 900°C. By running simple solid state reduction experiments, it is possible to simultaneously derive thermodynamic and diffusion data. In the range of non–stoichiometry we report, deviation from stoichiometry follows a power law of the oxygen partial pressure with a power law exponent of roughly $-1/4.5$. The OCV changes observed during the relaxation stage of reduction experiments in the solid state, are interpreted in terms of bulk redistribution of oxygen in the sample. These changes are modelled by solving Fick's second law with appropriate Von Neumann boundary conditions whence a chemical diffusion coefficient is derived. It is worth emphasising the fact that the method we describe is a relatively straightforward alternative either to relaxation experiments, for which there always remains some ambiguity as to the influence of surface exchange, or to impedance spectroscopy which provides a different, possibly greater range of information in regard to material properties but is also more complex to interpret.

In addition, we have subjected the sample to gas–phase redox perturbations. We show that under the conditions investigated, the kinetics of oxygen uptake by, or release from the sample are limited by the rate at which gas–solid oxygen exchange occurs at the sample surface, not by oxygen chemical diffusion in the bulk. Exchange coefficients are determined under different conditions and are shown to be mainly sensitive to the water vapour pressure.

Various lines of investigation are now being pursued. Regarding cerium oxide, we are currently studying a broader range of conditions in order to obtain temperature dependent vacancy diffusion coefficients and ascertain possible changes in diffusion properties as defects change from a doubly ionised to a singly ionised configuration. Characterising the impact of grain boundaries on oxygen diffusion in a chemical potential gradient also constitutes a topic of great interest and the device presented here is well suited to do so. Finally, other non–stoichiometric materials such as cation doped uranium oxides or uranium–cerium mixed oxides are also under investigation.

Acknowledgements: .

[1] W. C. Chueh, C. Falter, M. Abbott, D. Scipio, P. Furler, S. M. Haile, and A. Steinfeld, Science **330**, 1797 (2010), ISSN 0036-8075, https://science.sciencemag.org/content/330/6012/1797.full.pdf, URL https://science.sciencemag.org/content/330/6012/1797.

[2] H. Inaba and H. Tagawa, Solid State Ionics **83**, 1 (1996), ISSN 0167-2738, URL http://www.sciencedirect.com/science/article/pii/0167273895002294.

[3] C. Wagner, The Journal of Chemical Physics **21**, 1819 (1953), https://doi.org/10.1063/1.1698670, URL https://doi.org/10.1063/1.1698670.

[4] K. Kiukkola, Acta Chemica Scandinavica **16**, 327 (1962).

[5] B. Dorado, P. Garcia, G. Carlot, C. Davoisne, M. Fraczkiewicz, B. Pasquet, M. Freyss, C. Valot, G. Baldinozzi, D. Siméone, et al., Phys. Rev. B **83**, 035126 (2011).

[6] J. Fouletier, G. Vitter, and M. Kleitz, Journal of Applied Electrochemistry **5**, 111 (1975), ISSN 1572-8838, URL https://doi.org/10.1007/BF00613213.

[7] A. Caneiro, M. Bonnat, and J. Fouletier, Journal of Applied Electrochemistry **11**, 83 (1981), ISSN 1572-8838, URL https://doi.org/10.1007/BF00615326.

[8] J. Fouletier, H. Seinera, and M. Kleitz, Journal of Applied Electrochemistry **5**, 177 (1975), ISSN 1572-8838, URL https://doi.org/10.1007/BF01637267.

[9] P. Kofstad, *Nonstoichiometry, Diffusion, and Electrical Conductivity in Binary Oxides* (Accademic Press Inc. Publishers, 1960), 3rd ed.

[10] M. Patrakeev, I. Leonidov, and V. Kozhevnikov, Journal of Solid State Electrochemistry **15**, 931 (2011).

[11] R. Panlener, R. Blumenthal, and J. Garnier, Journal of Physics and Chemistry of Solids **36**, 1213 (1975), ISSN 0022-3697, URL http://www.sciencedirect.com/science/article/pii/0022369775901924.

[12] M. Mogensen, N. M. Sammes, and G. A. Tompsett, Solid State Ionics **129**, 63 (2000), ISSN 0167-2738, URL http://www.sciencedirect.com/science/article/pii/S0167273899003185.

[13] J. Philibert, *Atom movements: Diffusion and Mass transport in solids* (Editions de Physique, Les Ulis, France, 1991).

[14] J. J. Moré, in *Numerical Analysis*, edited by G. A. Watson (Springer Berlin Heidelberg, Berlin, Heidelberg, 1978), pp. 105–116, ISBN 978-3-540-35972-2.

[15] W. Sitte, E. Bucher, A. Benisek, and W. Preis, Spectrochimica Acta Part A: Molecular and Biomolecular Spectroscopy **57**, 2071 (2001), ISSN 1386-1425, URL http://www.sciencedirect.com/science/article/pii/S1386142501004899.

[16] I. Riess, M. Ricken, and J. Nölting, Journal of Solid State Chemistry **57**, 314 (1985), ISSN 0022-4596, URL http://www.sciencedirect.com/science/article/pii/0022459685901938.

[17] H. L. Tuller and A. Nowick, Journal of the Electrochemical society **126**, 209 (1979).

[18] I. Riess, H. Janczikowski, and J. Nölting, Journal of Applied Physics **61**, 4931 (1987), https://doi.org/10.1063/1.338363, URL https://doi.org/10.1063/1.338363.

[19] J. W. Dawicke and R. N. Blumenthal, Journal of The Electrochemical Society **133**, 904 (1986), URL https://doi.org/10.1149%2F1.2108760.

[20] G. J. VanHandel and R. N. Blumenthal, Journal of The Electrochemical Society **121**, 1198 (1974), URL https://doi.org/10.1149%2F1.2402012.

[21] W. Lai and S. M. Haile, Journal of the American Ceramic Society **88**, 2979 (2005), https://ceramics.onlinelibrary.wiley.com/doi/pdf/10.1111/j.1551-2916.2005.00740.x, URL https://ceramics.onlinelibrary.wiley.com/doi/abs/10.1111/j.1551-2916.2005.00740.x.

[22] S. Ackermann and J. R. Scheffe, The Journal of Physical Chemistry C **118**, 5216 (2014), URL https://pubs.acs.org/doi/10.1021/jp500755t.